Comparative study of crystallographic, spectroscopic, and laser properties of Tm^{3+} in $NaT(WO_4)_2$ (T = La, Gd, Y, and Lu) disordered single crystals

J. M. Cano-Torres, M. Rico, X. Han, M. D. Serrano, C. Cascales, and C. Zaldo*
Instituto de Ciencia de Materiales de Madrid, Consejo Superior de Investigaciones Científicas, c/ Sor Juana Inés de la Cruz 3, E-28049 Madrid, Spain

V. Petrov and U. Griebner
Max Born Institute for Nonlinear Optics and Short Pulse Spectroscopy, Max-Born-Strasse 2A, D-12489, Berlin, Germany

X. Mateos
Física i Cristal.lografia de Materials i Nanomaterials, Universitat Rovira i Virgili, Campus Sescelades, c/ Marcel.lí Domingo s/n, E-43007 Tarragona, Spain

P. Koopmann and C. Kränkel
Institut für Laser-Physik, Universität Hamburg, Luruper Chaussee 149, D-22761 Hamburg, Germany
(Received 11 July 2011; revised manuscript received 23 September 2011; published 10 November 2011)

Tetragonal double tungstate single crystals with formula $NaT(WO_4)_2$ have been grown by the Czochralski (T = Gd, La, Y) or by the top-seeded solution growth (T = Lu) methods with Tm concentration between 8×10^{18} and 7.85×10^{20} cm^{-3}. The spectroscopic properties of Tm^{3+} in these crystals are related with the peculiarities of their $I\bar{4}$ crystalline structure. Sixty-five percent of La ions in $NaLa(WO_4)_2$ are in the $2d$ site, while in the other crystal hosts, the lanthanide occupies preferentially the $2b$ site (59% in T = Gd, 74% in T = Y, and 58% in T = Lu). As a consequence, the linewidths of spectral bands associated with the electronic transitions are significantly narrower in $NaLa(WO_4)_2$ than in the rest of the isostructural crystals considered. Polarized spectroscopic measurements at 5 K and at higher temperatures, along with energy level simulation of the $4f^{12}$ configuration using a single-electron Hamiltonian, including free-ion and crystal field interactions, allowed us to determine the irreducible representation and energy of Stark levels up to the $^3P_0$ multiplet and thus to obtain realistic partition functions (Z) used for emission cross-section calculations. In particular, for the $^3F_4$(u) → $^3H_6$(l) laser transition at $\lambda \approx 2$ μm, this provides: $Z_l/Z_u = 1.436$ (T = Gd), 1.464 (T = La), 1.448 (T = Y), and 1.471 (T = Lu). Radiative lifetimes calculated by the Judd-Ofelt and Füchtbauer-Ladenburg methods are in agreement and decrease in the following order T = Gd, La, Y, and Lu, however, nonradiative losses are stronger for T = Gd and La crystals; therefore, experimental lifetimes of $^1D_2$, $^1G_4$, $^3H_4$, and $^3F_4$ Tm^{3+} multiplets do not change too much with crystal host. For 4.68 at.% Tm:$NaY(WO_4)_2$ crystal continuous-wave laser operation is obtained with ≈42% of slope efficiency and a record (for this crystal class) tuning capability of λ = 1847–2069 nm. The broad bandwidths, $\Delta\lambda_{FWHM} > 20$ nm, of the free-running laser emission are promising for ultrafast (fs) mode-locked laser operation near $\lambda \approx 2$ μm.

DOI: 10.1103/PhysRevB.84.174207 PACS number(s): 78.55.Qr, 61.66.Fn, 42.55.Rz

I. INTRODUCTION

Tm^{3+} solid-state lasers are of interest for different environmental, biomedical, and material processing applications based on vibronic molecular absorption around 2 μm. This emission range has been often covered by Ho^{3+} solid-state lasers pumped by discharge lamps in the blue and violet; however, modern laser technology relies on semiconductor diode lasers (DLs) for pumping and therefore efficient absorption in the near infrared (NIR) region (λ = 750–1000 nm) is desirable. Ho^{3+} fails to fulfill this requirement because the absorption cross section of the $^5I_5$ ($^{2S+1}L_J$) multiplet at $\lambda \approx 890$ nm is very weak, typically $\sigma_{ABS} \approx 1\text{-}5 \times 10^{-21}$ cm^2. Contrary to this, the $^3H_4$ Tm^{3+} multiplet has an order of magnitude larger σ_{ABS} at $\lambda \approx 800$ nm, which matches the emission of AlGaAs DLs. The $^3H_4$ Tm^{3+} de-excitation takes place through the intermediate $^3H_5$ and $^3F_4$ multiplets. If the dopant density is large enough, this de-excitation is accompanied by a cooperative Tm-Tm cross-relaxation, populating further the $^3F_4$ multiplet,[1] from which the $^3F_4$ → $^3H_6$ laser emission at λ∼1950 nm takes place. Note that these wavelengths, slightly shorter than the main emission band of Ho^{3+} lasers, correspond to increased water absorption, which is essential, e.g., for efficient tissue ablation applications.

Tm^{3+} also possesses other laser channels for which laser emission at room temperature has been achieved: $\lambda \approx 2300$ nm ($^3H_4$ → $^3H_5$),[2] $\lambda \approx 1580$ nm ($^1G_4$ → $^3F_3$),[3] $\lambda \approx 1500$ nm ($^3H_4$ → $^3F_4$),[4] $\lambda \approx 800$ nm ($^1G_4$ → $^3H_5$),[3] $\lambda \approx 650$ nm ($^1G_4$ → $^3F_4$),[3] $\lambda \approx 510$ nm ($^1D_2$ → $^3H_5$),[3] $\lambda \approx 486$ nm ($^1G_4$ → $^3H_6$),[5] and $\lambda \approx 450$ nm ($^1D_2$ → $^3F_4$).[3] Those related with $^1D_2$ and $^1G_4$ relaxations can be excited with NIR DLs by upconversion.[6] Moreover, Tm-Ho[7–9] and Yb-Tm[10] resonant transfers have been used to extend the emission and excitation spectral ranges and to enhance the efficiency of Tm-based solid-state laser systems. Detailed spectroscopic information on Tm^{3+} is therefore essential for understanding the complex Tm^{3+} laser dynamics and the properties of Tm-doped laser materials.

In contrast to other lasant lanthanides (like Nd^{3+}, Er^{3+}, or Ho^{3+}), the Tm^{3+} electronic transitions in crystals are broad due to the interaction of the $4f^{12}$ electrons with the lattice

vibrations of the host. The tuning capability of Tm^{3+} lasers operating in the continuous-wave (cw) regime has been shown in different ordered crystals, either oxides[11,12] or fluorides.[13] Host disorder in the crystals can contribute to enlarge this tuning range by introducing additional inhomogeneous broadening of the spectral lines of Tm^{3+}. Moreover, such disordered crystals are less sensitive to the matching between the laser crystal absorption and the pump DL emission, and the interionic interactions are promoted even at low ion densities due to the presence of some fraction of ion pairs. Gain media with broadband emission are also desirable for ultrashort (femtosecond) laser operation.

The tetragonal double tungstates (DW), with nominal formula $MT(WO_4)_2$ (hereafter MTW), where M and T are monovalent and trivalent ions, respectively, are a class of disordered crystals, which recently has attracted attention for tunable and femtosecond lasers. When doped with Yb^{3+}, pulses down to 53 fs at 1035 nm have been demonstrated using Yb:NaYW.[14] More recently, using Tm,Ho co-doped NaYW crystals laser pulses of 191 fs have been demonstrated at 2060 nm.[15] Although some previous spectroscopic and laser studies on Tm-doped NaTW crystals have been reported for T = La,[16,17] Gd,[18–20] Y,[21–24] and Lu,[25] to predict, model, and optimize the laser performance of such crystals, it is essential to assess the effect of the crystal host on the Tm^{3+} spectroscopic properties and to clarify the following uncertainties present in the published data: (i) *Crystal structure of the tetragonal DW hosts*. Although the $I\bar{4}$ space group was determined for NaTW with T = Gd, Y, and Lu, the crystallographic details for NaLaW remain uncertain. (ii) *Partition functions (Z)*. Partition functions are often used for the emission cross-section calculations, and the Z value is related to the relative energies of the Stark levels within a $^{2S+1}L_J$ multiplet. However, these energy level distributions are not well established. Some of the transitions between the Stark levels are forbidden in the S_4 point symmetry of the crystal sites occupied by Tm^{3+}. Therefore, in the low-temperature optical absorption and emission spectra, less bands should be observable than the number of excited Stark levels, although experimentally the inverse situation is found. (iii) *Polarization properties of observed bands*. A critical point for the correct understanding of the Tm^{3+} spectroscopic properties is to determine the irreducible representation (IR) of $^3H_6(0)$, which determines the expected band intensity for a given light polarization. (iv) *Lifetimes*. The $^3F_4$ laser relevant multiplet emits photons only by transition to the ground $^3H_6$ multiplet and therefore their lifetime measurement is affected by reabsorption.

In this work we present a crystallographic study of NaLaW and a comparison between the Tm^{3+} spectroscopy in the four isostructural disordered Na-based DW laser hosts, i.e., NaTW with T = La, Gd, Y, and Lu. The crystal cell volume decreases with smaller T^{3+} ionic radius of the passive eight-coordinated rare earth (1.16 Å for La^{3+}, 1.053 Å for Gd^{3+}, 1.019 Å for Y^{3+}, and 0.977 Å for Lu^{3+}),[26] and the Tm^{3+} spectroscopic properties are expected to change. Along with the determination of the different degree of disorder exhibited by these four crystals (as we shall show, NaLaW is significantly more ordered than the others), crystal field (CF) simulations have been carried out to determine a reliable list of energy levels and their IRs. The role of the Tm concentration on the fluorescence dynamics is considered in the four crystals. The present work also includes the first results of room-temperature laser operation for Tm-doped NaYW, both under Ti:sapphire and DL pumping, providing the largest spectral tuning ranges for this crystal class so far reported.

II. CRYSTAL GROWTH

NaTW crystals with T = Tm and Lu melt with decomposition, while crystals with T = La, Gd, and Y melt congruently. Therefore, NaLaW, NaGdW, and NaYW crystals were grown by the Czochralski method, while the top-seeded solution growth (TSSG) method without pulling was used for NaLuW. Because the incorporation of Tm modifies the melting properties for the T = Y, La, and Gd crystals, an upper limit (10–15 at.%) of Tm concentration in the melt was found to obtain Czochraski-grown defect-free crystals.

For each host, we grew crystals exhibiting three Tm doping levels. (a) A low level, typically 0.2 at.% in the melt. These samples have been used to study the radiative properties of isolated Tm^{3+} ions. (b) An intermediate Tm doping level, i.e., 5 at.% in the melt was used for optimized laser operation. (c) Crystals with a high Tm doping level, i.e., 7–10 at.% were used to explore the upper limit of Tm incorporation by the Czochralski method and to study Tm-Tm interactions. Finally, Tm-doped NaTW powders prepared by solid-state reaction were used exclusively for $^3F_4$ lifetime measurement purposes.

The Tm concentration in the grown crystals was measured by x-ray emission spectrometry for the intermediate and high Tm doping levels. Details of this procedure have been given previously.[27] The Tm concentrations for the low doping level were calculated by comparison of the integrated optical absorption with that at higher doping levels. The Tm density ([Tm]) was calculated using the lattice parameter of the corresponding undoped host crystal. Table I summarizes the Tm concentration of the used crystals.

TABLE I. Tm concentration of the Tm:Na$T(WO_4)_2$ crystals under study.

Tm:NaLaW			Tm:NaGdW			Tm:NaYW			Tm:NaLuW		
Melt	Crystal		Melt	Crystal		Melt	Crystal		Melt	Crystal	
(at.%)	(at.%)	(10^{20} cm^{-3})	(at.%)	(at.%)	(10^{20} cm^{-3})	(at.%)	(at.%)	(10^{20} cm^{-3})	(at.%)	(at.%)	(10^{20} cm^{-3})
0.2	0.08	0.05	0.2	0.09	0.06	0.2	0.14	0.09	≈0.7	0.76	0.51
5	2.52	1.50	5	3.7	2.34	5	4.68	3.07	5	5.67	3.80
10	3.6	2.20	7	4.8	3.07	7.9	7.67	5.03	10	11.71	7.85

TABLE II. Room-temperature lattice parameters of $NaT(WO_4)_2$ (T = La, Gd, Y, and Lu) single crystals. Na/T occupancy factors (OF), Na/T bond length to oxygens, average bond length ($\bar{R}$) and distortion degree (Δ) of TO_8 polyhedra for the 2*d* (1) and 2*b* (2) sites.

Structural parameter	NaLaW	NaGdW	NaYW	NaLuW
$a = b$ (Å)	5.3575(7)	5.2440(5)	5.2014(4)	5.1692(3)
c (Å)	11.671(2)	11.3794(14)	11.2740(12)	11.1832(15)
2*d* OF, Na(1)/T(1)	0.35(3)/0.65(3)	0.55(2)/0.45(2)	0.67(1)/0.33(1)	0.57(1)/0.43(1)
2*b* OF, Na(2)/T(2)	0.63(3)/0.37(3)	0.41(2)/0.59(2)	0.26(1)/0.74(1)	0.42(1)/0.58(1)
Na(1)/T(1)-O(1) bond length (Å) × 4	2.51(3)	2.461(16)	2.438(15)	2.408(13)
Na(1)/T(1)-O(2) bond length (Å) × 4	2.56(3)	2.457(12)	2.414(14)	2.395(15)
$\bar{R}(1)$ (Å)	2.535	2.459	2.426	2.401
$\Delta(1) \times 10^3$	0.0973	0.0007	0.0245	0.0074
Na(2)/T(2)-O(1) bond length (Å) × 4	2.58(3)	2.478(13)	2.453(18)	2.441(16)
Na(2)/T(2)-O(2) bond length (Å) × 4	2.51(3)	2.450(16)	2.420(17)	2.405(15)
$\bar{R}(2)$ (Å)	2.545	2.464	2.436	2.423
$\Delta(2) \times 10^3$	0.1891	0.0323	0.0459	0.0552

The crystals were oriented by Laue x-ray diffraction method and then cut and polished for the spectroscopic studies and laser experiments.

III. STRUCTURAL CHARACTERIZATION

The crystalline structure of NaTW (T = Gd, Y, and Lu) single crystals has been reported in previous publications.[28,29] A similar room-temperature x-ray diffraction (XRD) study has been carried out now for the NaLaW single crystal. The objective of this study was (i) to determine the possible distortion of the crystal symmetry of NaLaW from the centrosymmetric space group (SG) $I4_1/a$ (No. 88) to the noncentrosymmetric $I\bar{4}$ (No. 82), in the same way as already established for T = Gd, Y and Lu[28,29] as well as for the related NaBiW[30] single crystals, and (ii) to estimate the local disorder associated with the shared occupation of the site (or sites) available in the actual SG symmetry of NaLaW by both monovalent Na^+ and trivalent $T^{3+}(Tm^{3+})$ cations. Detailed explanations of procedures and results for these analyses can be found in the Supplementary Material (SM) Sec. I.[31]

Regarding the first point, the measurement of the individual intensities of systematic absences exceptions forbidden by the presence of a 4_1 axis (00ℓ with ℓ even but $\ell \neq 4n$) and by a a plane ($h\bar{h}0$, with $h \neq 2n$), undoubtedly indicates that NaLaW is only adequately described by the symmetry characteristics of the noncentrosymmetric SG $I\bar{4}$, similarly to the other previously studied NaTW crystals. However, it is worth mentioning that the most intense reflections characterizing the $I4_1/a \rightarrow I\bar{4}$ distortion, namely *002* and $1\bar{1}0$ for the 4_1 axis and the a plane, respectively, have relative intensities considerably higher than for the other crystals of the NaTW family studied, compare data in the SM (Table SM1)[31] and those in Table I for NaGdW[28] and in Table II for NaBiW,[30] of the corresponding references. From the 15 systematic absence exceptions found with intensity $I > 2\sigma(F)$, five appear above the threshold $I > 3\sigma(F)$, and thus they have been retained for the refinement. The details and results of this refinement can be found in the SM (Table SM2).[31] Here, Table II only shows a comparison of some structural parameters for the four NaTW (T = La, Gd, Y, Lu) crystals relevant for the following discussion of their spectroscopic properties.

Concerning the second objective, it can be seen that the Na^+ and La^{3+} distribution described by the occupancy factors (OFs) does not correspond to the statistical one over both 2*b* and 2*d* S_4 sites. In crystals grown by the Czochralski method (T = La, Gd, Y), a Na^+ deficiency is found (the sum of the OFs reported in Table II for Na^+ in both sites is less than 1), due to its evaporation from the melt, which is compensated with extra incorporation of T^{3+} ions. However, NaLuW crystals grown by the TSSG method have a composition very close to the nominal one because of the Na^+ reservoir provided by the $Na_2W_2O_7$ flux during the growth.

The local disorder in the tetragonal NaTW crystals can be explained by the short-range (up to ~4 Å) Na/T distribution, i.e., the second shell of cations, around each of the two 2*b* and 2*d* S_4 sites. A multiple but yet finite number of these cationic distributions (or environments) around Tm^{3+} can be envisaged, which adopt symmetries ranging from S_4 (when neighbor cations are of the same nature, 4Na or 4T) to lower C_2 (for some specific 2Na/2T arrangements) or C_1 (for remaining 2Na/2T and for 3Na/1T or 3T/1Na environments), thus giving rise to locally different CF potentials and consequently to the characteristic broadening of optical bands even at low temperature. Obviously the most disordered situation is associated with OFs for Na/T equal to 0.5/0.5 for the two crystal sites.

From current data, it can be concluded that the NaLaW crystal is singular from the structural point of view: (i) It presents a higher degree of $I4_1/a \rightarrow I\bar{4}$ distortion; (ii) the preferred site for T^{3+} is 2*d,* while in NaGdW, NaYW, and NaLuW, this is 2*b*; (iii) it is a considerably ordered host because the OFs for Na/La largely deviate from the random 0.5/0.5 OFs for the two crystal sites; (iv) the T-O bond lengths are not only larger than in the three other crystals, but more important, the distortion of the two TO_8 polyhedra calculated as $\Delta = 1/8 \sum(\frac{R_i - \bar{R}}{\bar{R}})^2$ (R_i: individual bond length in each TO_8 polyhedron, $\bar{R}$: average bond length)[32] is by far the most significant in the NaTW family.

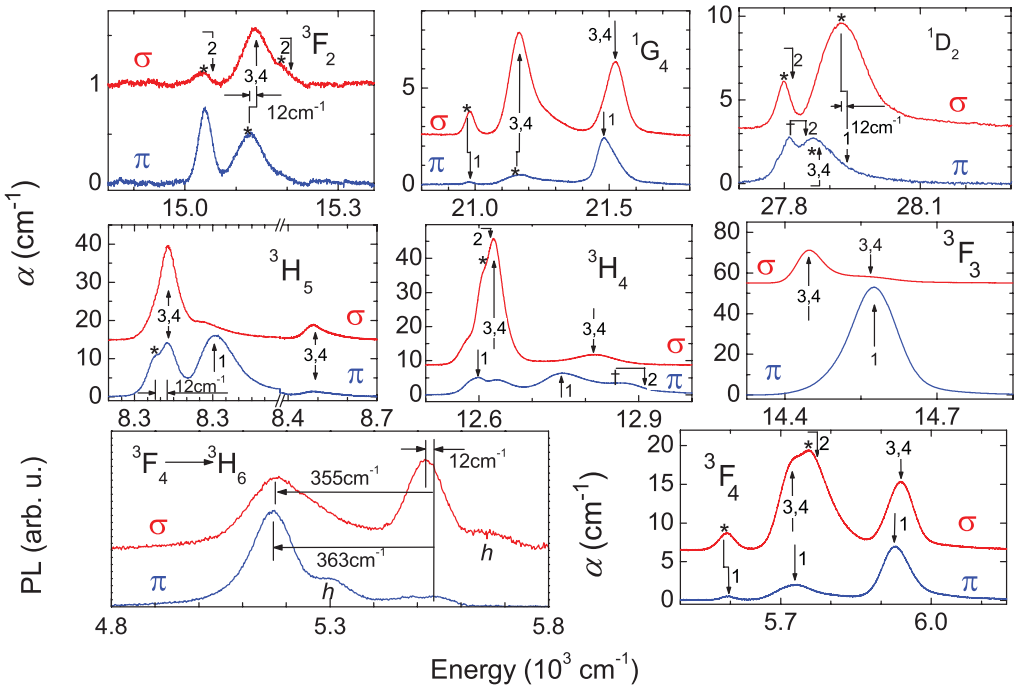

FIG. 1. (Color online) Polarized 5-K optical absorption (α) and PL of Tm-doped $NaY(WO_4)_2$ single crystal. The energy of the $^{2S+1}L_J(n')$ excited Stark levels are indicated by vertical arrows, and their Γ_1, Γ_2 and $\Gamma_{3,4}$ IR are abbreviated as 1, 2 and 3,4. Bands corresponding to transitions from the $^3H_6(1)$ and $^3H_6(2)$ levels are indicated by * and †, respectively. PL *hot* bands starting from excited $^3F_4(n \neq 0)$ levels are marked as h. σ spectra have been shifted arbitrary to give clarity to the figure.

IV. SPECTROSCOPIC CHARACTERIZATION

A. Energy levels of Tm^{3+}

The Tm^{3+} energy level scheme in the four used hosts was studied by low temperature (5–300 K) optical absorption (OA) and photoluminescence (PL) measurements. In both cases a closed-cycle He cryostat was used to control the sample temperature. OA was recorded in a Varian 5E spectrophotometer. The PL was excited with a Ti:sapphire laser and the emission, dispersed by a SPEX 340E spectrometer ($f = 34$ cm), was recorded with a 77-K cooled InSb photovoltaic detector (Hamamatsu, model P5968-060) connected to a lock-in amplifier. The OA and PL spectra are labeled as α ($\boldsymbol{E}\perp\mathbf{c}$ and $\boldsymbol{B}\perp\mathbf{c}$), σ ($\boldsymbol{B}//\mathbf{c}$), and π ($\boldsymbol{E}//\mathbf{c}$).

Figure 1 shows the polarized 5 K $^3H_6 \rightarrow {}^{2S+1}L_J$ OA and $^3F_4 \rightarrow {}^3H_6$ PL of Tm-doped NaYW crystals. In the four crystal hosts, the α and σ OA spectra were very similar, therefore α-spectra are not shown for the sake of brevity. OA results are used for the determination of the energy of Stark levels $^{2S+1}L_J(n')$ of excited multiplets relative to $^3H_6(0)$, whereas the PL results provide information on $^3H_6(n)$ Stark levels. Previously published PL results on the other three NaTW compounds, $T =$ La,[16] Gd,[18] and Lu,[25] included in some cases *hot* bands due to the heating of the sample by the Ti:sapphire laser excitation, and in few cases the OA assignments have been reconsidered; therefore, a full set of corrected 5 K OA and PL spectra are included now as SM; see Figs. SM1 (for $T =$ La), SM2 (for $T =$ Gd), and SM3 (for $T =$ Lu).[31]

The analysis of these spectra indicates that optical transitions retain well-defined S_4 polarization character with respect to the principal axes of the matrix. Consequently, the CF analysis can be reasonably performed with the symmetry characteristics of an average S_4 potential, whereas residual peaks appearing in the polarized spectra could be allowed transitions for Tm^{3+} centers with symmetry lower than S_4.

Table III shows the selection rules expected for electric dipole (ED) and magnetic dipole (MD) transitions in S_4 symmetry. It is worth noting that $\Gamma_1 \rightarrow \Gamma_1$ and $\Gamma_2 \rightarrow \Gamma_2$ ED transitions as well as $\Gamma_1 \leftrightarrow \Gamma_2$ MD transitions are forbidden. This fact, together with the band overlapping associated with different Na/T environments for each of the two Tm sites and the presence of $^3H_6(n \neq 0)$ level absorption contributions make the interpretation of the Tm^{3+} spectroscopy only on an empirical basis uncertain. The comparison of the Tm spectroscopic results in the four isostructural crystals helps to clarify some doubts: (i) The larger band gap of NaLuW allows one to observe the $^3H_6(0) \rightarrow {}^3P_0$ ED transition in π polarization; see Fig. SM3.[31] Since this $^3P_0$ singlet level has

TABLE III. Selection rules for ED and MD transitions in S_4 symmetry.

S_4/ED	Γ_1	Γ_2	$\Gamma_{3,4}$
Γ_1	–	π	α,σ
Γ_2	π	–	α,σ
$\Gamma_{3,4}$	α,σ	α,σ	π
S_4/MD	Γ_1	Γ_2	$\Gamma_{3,4}$
Γ_1	σ	–	α,π
Γ_2	–	σ	α,π
$\Gamma_{3,4}$	α,π	α,π	σ

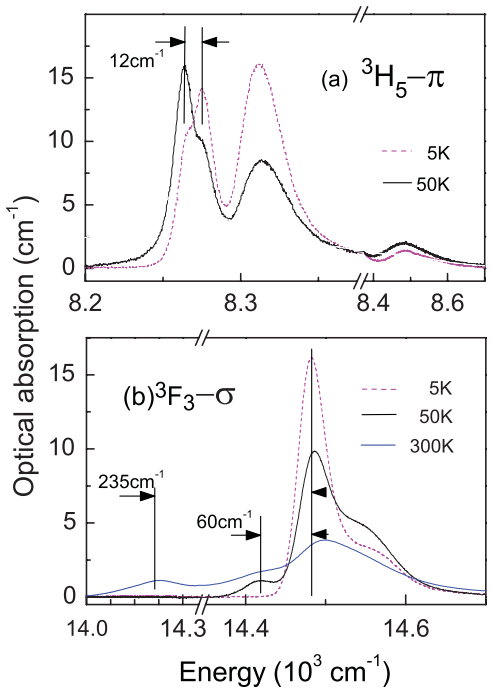

FIG. 2. (Color online) Selected ground state absorption transitions in Tm-doped $NaY(WO_4)_2$ ([Tm] = 3.07×10^{20} cm^{-3}) measured at several temperatures. (a) $^3H_6 \rightarrow {}^3H_5$ π-polarized absorption. (b) $^3H_6 \rightarrow {}^3F_3$ σ-polarized absorption.

Γ_1 IR, the IR of $^3H_6(0)$ must be Γ_2. (ii) The OA and PL of Tm^{3+} in NaLaW have smaller bandwidths than in the other hosts considered, for instance, the full width at half maximum (FWHM) of the $^3F_3$ π-polarized absorption amounts to 44, 70, 73, and 76 cm^{-1} for T = La, Gd, Y, and Lu, respectively; therefore, Tm^{3+} bands overlapping in NaTW (T = Gd, Y, and Lu) appear well resolved in NaLaW, see, for instance, the comparison of the 5 K $^3H_5$ OA shown in the SM (Fig. SM4).[31]

Information on the Stark splitting of the ground $^3H_6$ multiplet can be further inferred from the thermal evolution of the OA. Figure 2 shows such results only for the Tm-doped NaYW crystal, but similar data were collected for the four crystal hosts. The π-polarized $^3H_5$ OA is well suited for the determination of the energy of the $^3H_6(1)$ level because the observed bands are sharp, and the MD contributions allow one to observe $^3H_6 \rightarrow {}^3H_5$ transitions in all polarizations. The band observed around 8275 cm^{-1} shows at 5 K a low-energy shoulder. The intensity of this shoulder increases upon heating up to 50 K and decreases at higher temperatures, whereas the intensity of the main 8275 cm^{-1} band decreases monotonically upon heating. This is due to the redistribution of the electronic population between $^3H_6(n)$ Stark levels upon increasing temperature. The energy difference between these two OA bands, 12 cm^{-1}, is ascribed to the first excited level, i.e., $^3H_6(1)$. The energy of the $^3H_6(2)$ and $^3H_6(3)$ levels is better resolved in the σ-polarized $^3F_3$ OA thermal evolution. In that case, as the terminal $^3F_3(0)$ level has a $\Gamma_{3,4}$ IR (see later Table IV), the selection rules from levels with Γ_1 and Γ_2 IRs are the same, and all $^3H_6(0,2,3) \rightarrow {}^3F_3(0)$ ED transitions are observed in the σ-polarized spectrum. Table IV summarizes the observed energies (E_o) for Tm^{3+} in the four crystal hosts studied and Fig. SM5[31] shows a scheme of Tm^{3+} energy levels in NaTW crystals.

The above conclusion about the $^3H_6(0)$ IR is in agreement with that found in Tm-doped $CaWO_4$ crystals with scheelite structure.[33] Nevertheless, the determination of the energy scheme of Stark levels from low-temperature measurements was assisted by an initial CF simulation[34] using CF parameters extrapolated from those of Er^{3+} in the isostructural NaBiW crystal[35] and Tm^{3+} free-ion (FI) parameters determined earlier.[36] The procedures for these calculations have been described in earlier work.[37] The full rationalization and assignment of observed transitions has been made possible through the present combination of experimental and simulation results. The calculations yielded energy values compatible with the experimental results only when Γ_2 is the IR of $^3H_6(0)$. This simulation and energy level refinement produced the full list of calculated Tm^{3+} Stark level energies (E_c) summarized in Table IV for the four crystal hosts considered by using the CF parameters indicated in Table V. From these Stark level energy lists the partition function of each multiplet was obtained using E_c values when E_o was not observed.

B. Radiative properties of Tm^{3+}

Judd-Ofelt analysis. The Judd-Ofelt (JO) theory[38,39] allows one to quantify the radiative properties of trivalent lanthanides in condensed matter from their optical absorption. Previous JO analyses of Tm^{3+} in DW have been provided by other authors in NaTW, T = La,[17] Gd,[20,40] Y,[21–24] and Bi;[41] however, the significance of the variations found for isostructural hosts is difficult to assess because of the differences in methodology and accepted uncertainties: In some works the thulium concentration in the crystal has not been known with certainty,[21–23] often a constant average refractive index has been assumed,[21–23,40,41] whereas in other cases the $^1D_2$[41] or magnetic dipole[24,40,41] absorption contributions have been ignored, in certain cases crystal orientation or the spectrum labelling is obviously wrong,[17,40] and finally some works average the crystal anisotropy over the absorption probabilities,[17,40,41] although others over Ω_k parameters.[20,24] As result of this, the radiative lifetimes calculated for the $^3F_4$ multiplet vary from 1011 to 2476 μs and for the $^3H_4$ multiplet from 178 to 373 μs. In the present work, we apply the same methodology to the four crystals considered, using the actual thulium concentrations in the crystal given in Table I, the true refractive indices (including spectral dispersion) determined in our previous works on NaTW crystal properties, T = La,[42] Gd,[28] Y,[14] and Lu,[43] and now extended up to $\lambda \approx 2$ μm, including $^1D_2$ and MD contributions. In this way it is expected that the relative variations obtained become significant. Details of our JO calculation procedures can be found in our previous works.[30,44] Here we just describe the most relevant results of the JO analysis.

Figure 3 shows the evolution of the measured integrated OA cross section, $\Gamma/[Tm] = [Tm]^{-1}\int\alpha(\lambda)d\lambda$, with the crystal host. Despite the isomorphism of the four NaTW crystals here considered, systematic increase of the integrated OA cross section is found in the sequence T = Gd $\rightarrow$ La $\rightarrow$ Y $\rightarrow$ Lu. The last two, despite the very similar lattice parameters, exhibit significant differences. Table SM2[31] includes the corresponding polarization averaged, $(2\sigma+\pi)/3$, ED oscillator strengths,

$\bar{f}_{ED,ex}$, and the fitted JO parameters sets, $\Omega_{k=2,4,6}$. The radiative properties from $^1D_2$ to $^3F_4$ multiplets are obtained from these Ω_k sets. Table VI shows the most relevant radiative properties of multiplets with laser transitions. A full list of radiative properties can be found in the SM; see Table SM3.[31] The JO calculated radiative lifetimes of all Tm^{3+} multiplets decrease in the same crystal host sequence as Γ/[Tm] increases; see Tables VI and SMIII.[31]

Füchtbauer-Ladenburg analysis. The radiative lifetime of a given $^{2S+1}L_J$ multiplet can be alternatively calculated by using the Füchtbauer-Ladenburg (FL) expression,[45]

$$\tau_{r,J}^{-1} = 8\pi c \times \sum_{J'} n_{J'}^2 \int \frac{\langle \sigma_{EMI}(\lambda) \rangle_{J'}}{\lambda^4} d\lambda, \quad (1)$$

where $\langle \sigma_{EMI} \rangle_{J'}$ is the averaged over polarization emission cross section of the $J \rightarrow J'$ transition.

TABLE IV. 5 K observed (E_o) and calculated (E_c) energy levels (cm^{-1}) of Tm^{3+} in $NaT(WO_4)_2$ (T = La, Gd, Y, and Lu) single crystals. $\|$ indicates the observed polarization of the OA or PL transitions and IR are the level irreducible representations Γ_1, Γ_2, and $\Gamma_{3,4}$, abbreviated as 1, 2 and 3,4, respectively. Z is the partition function.*,† Transitions observed from the first $^3H_6(1)$ ($\Gamma_{3,4}$) and second $^3H_6(2)$ (Γ_1) excited energy levels, respectively.

			Tm:NaLaW			Tm:NaGdW			Tm:NaYW			Tm:NaLuW		
$^{2S+1}L_J$	$\|$	IR	E_o	E_c	Z	E_o	E_c	Z	E_o	E_c	Z	E_o	E_c	Z
$^3H_6$		2	0	−6	5.753	0	−1	5.610	0	−4	5.580	0	−3	5.507
	πOA$^3H_5$	3,4	10	9		13	16		12	17		14	21	
	σOA$^3F_3$	1	35	26		56	31		60	36		65	43	
	σOA$^3F_3$	2	241	249		253	251		235	242		266	273	
		2	–	304		–	278		–	274		–	273	
		1	–	305		–	315		–	322		–	331	
		3,4	–	306		–	314		–	321		–	334	
	σPL$^3F_4$	3,4	334	348		345	353		355	366		335	334	
		1	–	347		–	361		–	372		–	386	
	πPL$^3F_4$	2	370	368		354	372		363	383		358	390	
$^3F_4$	π	1	5605	5605	3.930	5599	5593	3.907	5595	5583	3.853	5591	5580	3.742
($^1G_4$)	α,σ	3,4	5742	5736		5725	5732		5722	5726		5724	5724	
	π	1	5728	5739		5730	5736		5729	5733		5730	5757	
	*α,σ	2	5780	5773		5772	5778		5768	5774		5771	5777	
		2	–	5910		–	5902		–	5916		–	5933	
	π	1	5911	5909		5926	5914		5927	5914		5933	5913	
	α,σ	3,4	5918	5922		5933	5933		5938	5936		5947	5941	
$^3H_5$		2	–	8265		–	8279		–	8279		–	8283	
	α,σ,π	3,4	8259	8267		8273	8283		8275	8286		8279	8290	
	π	1	8283	8274		8305	8291		8312	8296		8319	8302	
	α,σ,π	3,4	8464	8485		8473	8479		8484	8476		8491	8478	
		2	–	8481		–	8511		–	8519		–	8527	
		1	–	8502		–	8509		–	8515		–	8526	
		3,4	–	8503		–	8520		–	8528		–	8537	
		1	–	8521		–	8529		–	8538		–	8552	
$^3H_4$	π	1	12596	12587	5.560	12597	12608	5.452	12599	12606	5.451	12599	12614	5.356
($^3F_4$)	*α,σ	2	12613	12606		12616	12621		12619	12616		12621	12614	
	α,σ	3,4	12621	12626		12625	12634		12628	12636		12630	12642	
	π	1	12763	12755		12755	12746		12754	12744		12757	12747	
		1	–	12803		–	12787		–	12792		–	12797	
	α,σ	3,4	12790	12804		12813	12817		12814	12824		12829	12837	
	†π	2	12880	12870		12919	12896		12917	12898		12921	12898	
$^3F_3$	α,σ	3,4	14473	14477		14481	14485		14481	14491		14487	14496	
		2	–	14503		–	14514		–	14517		–	14520	
	α,σ	3,4	14548	14549		14556	14550		14563	14558		14568	14564	
		2	–	14554		–	14557		–	14563		–	14566	
	π	1	14567	14566		14569	14571		14568	14574		14570	14575	
$^3F_2$	*α,σ	2	15034	15034		15046	15043		15046	15054		15047	15057	
	α,σ	3,4	15139	15138		15133	15135		15136	15145		15139	15149	
	*α,σ	2	–	15147		–	15162		15198	15178		15195	15186	
		1	–	15210		–	15209		–	15220		–	15226	

TABLE IV. *(Continued)*

		IR	Tm:NaLaW			Tm:NaGdW			Tm:NaYW			Tm:NaLuW		
$^{2S+1}L_J$	‖	Γ	E_o	E_c	Z	E_o	E_c	Z	E_o	E_c	Z	E_o	E_c	Z
$^1G_4$	π	1	21013	21022	2.921	20999	20996	2.866	20980	20986	2.701	20979	20985	2.645
($^3H_4$)	α,σ	3,4	21175	21184		21167	21174		21163	21171		21164	21174	
	$^*\alpha,\sigma$	2	21234	21235		–	21236		–	21236		–	21245	
	π	1	21310	21303		–	21280		–	21279		21290	21286	
	$^*\alpha,\sigma$	2	21456	21448		–	21435		–	21459		–	21489	
	π	1	21485	21485		21477	21481		21482	21484		21490	21490	
	α,σ	3,4	21502	21500		21516	21508		21522	21515		21527	21529	
$^1D_2$	$^*\alpha,\sigma$	2	27814	27819	3.490	27813	27817	3.648	27809	27805	3.814	27805	27811	3.555
($^3P_2$)	$^\dagger\pi$	2	27851	27860		27860	27860		27848	27853		27874	27861	
	$^*\pi$	3,4	27927	27931		27899	27917		27877	27905		27898	27911	
	$^*\alpha,\sigma$	1	27963	27946		27947	27927		27937	27911		27927	27916	
$^1I_6$		2	–	34573		–	34559		–	34498		–	34453	
	α,σ	3,4	–	34592		–	34575		–	34513		34486	34466	
	π	1	–	34621		–	34601		–	34534		34464	34484	
		1	–	34790		–	34754		–	34689		–	34642	
		3,4	–	34881		–	34856		–	34789		–	34741	
		2	–	34932		–	34943		–	34895		–	34961	
		1	–	34967		–	34967		–	34920		–	34887	
		3,4	–	34993		–	34980		–	34930		–	34896	
		2	–	35239		–	35186		–	35120		–	35082	
		2	–	35242		–	35188		–	35125		–	35087	
$^3P_0$	π	1	–	35352		–	35378		–	35281		35254	35256	

When J′ is the ground state $^3H_6$ multiplet, σ_{EMI} can be obtained from the absorption cross section, $\sigma_{ABS} = \alpha/[Tm]$, by the reciprocity method[46] as

$$\sigma_{EMI} = \sigma_{ABS}\frac{Z_l}{Z_u}e^{(E_{zl}-h\nu)/k_BT}, \quad (2)$$

where E_{zl} is the zero line ($0 \rightarrow 0'$) energy, and Z_l, Z_u are the partition function of the lower and upper multiplets, respectively, both obtained from the Stark energy levels of Table IV, and k_BT is the product of the Boltzmann constant (k_B) and the sample temperature ($T = 300$ K).

If J′ is not the ground state multiplet, the σ_{EMI} calculated by the reciprocity method is taken as a reference, σ_{EMI}^{REF}, for the calculation of the J → J′ emission cross section as

$$\sigma_{EMI}(\lambda) = \sigma_{EMI}^{REF}\frac{I\lambda^5}{I_{REF}\lambda_{REF}^5}, \quad (3)$$

where I and I_{REF} are the PL intensities at λ and λ_{REF}, respectively.

Room-temperature OA and PL spectra were collected for the four Tm-doped NaTW crystals considered. Results are not shown for the sake of brevity, but representative spectra for Tm:NaYW can be found in the SM; see Figs. SM6–SM10.[31] For a given $^{2S+1}L_J$ multiplet, the most critical points for this evaluation were to take into account the equipment spectral correction, to correlate the emission intensity in different spectral ranges, to discriminate and quantify overlapped fluorescence from lower lying multiplets (relevant for the $^1G_4$ fluorescence), and to properly account the σ_{EMI}^{REF} value calculated by reciprocity. For the latter, samples with the lowest available Tm concentration and the reciprocity σ_{EMI} value of the relative maximum at the longest wavelength were used.

TABLE V. S_4 CF parameters (CFps, in cm^{-1}) for Tm^{3+} in $NaT(WO_4)_2$ (T = La, Gd, Y, and Lu) laser crystals. Values in parentheses refer to estimated standard deviations in the indicated parameter.

CFps[a]	Tm:NaLaW	Tm:NaGdW	Tm:NaYW	Tm:NaLuW
B_0^2	404(14)	341(14)	323(15)	318(13)
B_0^4	−585(22)	−649(27)	−674(29)	−704(27)
B_4^4	±753(15)	±800(19)	±835(20)	±868(17)
B_0^6	−112(26)	−156(34)	−117(38)	−56(36)
B_4^6	±424(19)	±493(20)	±481(22)	±458(22)
iB_4^6	±340(28)	±186(61)	±265(47)	±300(37)
σ	10.0	12.6	14.9	14.1

[a]Phenomenological free-ion parameters obtained in S_4 fits (cm^{-1}) for T = La, Gd, Y, Lu: E^0 = 17585(1), 17568(2), 17597(2), 17627(2); E^1 = 6757(3), 6735(3), 6739(4), 6731(3); E^2 = 33.69(2), 33.63(2), 33.68(2), 33.67(2); E^3 = 673.6(2), 674.0(2), 670.6(3), 669.2(2); α = 16.70(6), 17.27(7), 15.51(8), 14.08(6); β = [−651]; γ = [1810]; ζ = 2633.6(8), 2632(1), 2634(1), 2635(1); M^0 = [4.00], [4.20], [4.15], [4.00], $M^2 = [0.56M^0]$, $M^4 = [0.32M^0]$; P^2 = [700], [590], [675], [700], $P^4 = [0.75P^2]$, $P^6 = [0.5P^2]$. Here, values in brackets were the same for the four crystals, and they were not varied through the fit of the energy levels in each case. $\sigma = [\sum(\Delta_i)^2/(L-p)]^{1/2}$, $\Delta_i = E_o - E_c$, L number of levels, p number of parameters included in the fit.

TABLE VI. Selected transition wavelengths, λ (nm), ED, and MD, radiative transition probabilities, A_{ED} and A_{MD} (s^{-1}), branching ratios, β (%), and radiative lifetimes, τ_r (μs), of Tm^{3+} in NaT(WO_4)$_2$ crystals calculated from the corresponding Ω_k (10^{-20} cm^2) sets: $\Omega_2 = 10.32$, $\Omega_4 = 2.55$, and $\Omega_6 = 1.19$ for Tm:NaLaW, $\Omega_2 = 9.48$, $\Omega_4 = 1.28$, and $\Omega_6 = 1.36$ for Tm:NaGdW, $\Omega_2 = 11.43$, $\Omega_4 = 2.64$, and $\Omega_6 = 1.42$ for Tm:NaYW and $\Omega_2 = 13.42$, $\Omega_4 = 3.51$, and $\Omega_6 = 1.52$ for Tm:NaLuW. The τ_r calculated by the FL method are also included with italics characters. See the SM[31] for a complete version of this table.

		Tm:NaLaW			Tm:NaGdW			Tm:NaYW			Tm:NaLuW		
$J \rightarrow J'$	λ	A_{ED+MD}	β_{ij}	τ_r	A_{ED+MD}	β_{ij}	τ_r	A_{ED+MD}	β_{ij}	τ_r	A_{ED+MD}	β_{ij}	τ_r
$^1D_2 \rightarrow {}^3H_4$	658	21743	31	14	20955	34	16	25283	31	12	31337	30	9.6
$^3F_4$	452	18816	26		19164	31		22074	27		26929	26	
$^3H_6$	363	22455	32		14097	23		24541	30		33580	33	
$^1G_4 \rightarrow {}^3H_5$	775	1700	17	99	1839	19	102	2046	17	85	2426	17	69
$^3F_4$	648	4374	43	*90*	4502	46	*78*	5176	44	*73*	6267	43	*66*
$^3H_6$	480	3809	38		3307	34		4351	37		5555	38	
$^3H_4 \rightarrow {}^3H_6$	811	3744	89	237	3703	89	241	4402	89	202	5390	89	165
				260			*267*			*211*			*174*
$^3F_4 \rightarrow {}^3H_6$	1853	640	100	1563	559	100	1790	720	100	1390	926	100	1080
				1779			*1800*			*1450*			*1179*

The FL method could not be applied to the $^1D_2$ multiplet because the $^1D_2 \rightarrow {}^3H_6$ PL could not be resolved from the tail of the excitation light. Radiative lifetimes calculated for $^1G_4$, $^3H_4$, and $^3F_4$ multiplets are given in Table VI for Tm:NaTW (T = La, Gd, Y, and Lu) crystals.

Experimental determination of the radiative lifetime. In order to assess the validity of the previous JO and FL radiative lifetime calculations, a comparison with experimental results is required. Experimental results of Tm^{3+} lifetimes in DWs have been reported in several works, but in all cases the data correspond to room-temperature measurements on samples with high Tm concentration (>0.5 × 10^{20} cm^{-3}). However, the experimental lifetime of a multiplet is related to its radiative lifetime as $\tau_{exp}^{-1} = \tau_r^{-1} + \tau_{ph}^{-1} + \tau_C^{-1}$, where τ_{ph}^{-1} and τ_C^{-1} are the multiphonon and energy transfer nonradiative probabilities. Therefore, possible thermal and Tm-Tm interactions, contributing to shorten the lifetime, and the reabsorption of the $^3F_4 \rightarrow {}^3H_6$ emission, contributing to enlarge it, have been so far ignored.

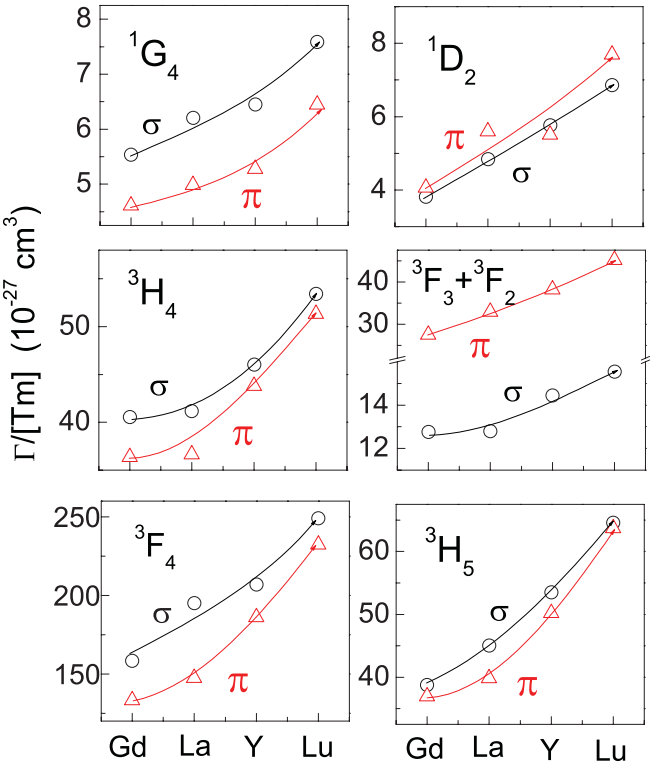

FIG. 3. (Color online) Comparison of the room-temperature Tm^{3+} integrated optical absorption cross sections, Γ/[Tm], of Tm:NaT(WO_4)$_2$ (T = La, Gd, Y, and Lu) crystals.

All these aspects are now addressed by the experimental determination of the lifetime of Tm^{3+} emissions using exclusively the samples with the lowest available Tm concentration, i.e., 0.2 at.% Tm-doped NaTW (T = La, Gd, and Y) single crystals, and a 0.1 at.% Tm-doped NaLuW polycrystalline material prepared by solid-state reaction. Resonant excitation was made for the $^1D_2$ (λ_{EXC} = 359 nm), $^1G_4$ (λ_{EXC} = 472 nm), and $^3H_4$ (λ_{EXC} = 796 nm) multiplets, while $^3F_4$ was excited through the $^3H_4$ multiplet. Details of the experimental techniques can be found in Sec. V of the SM.[31] For all these samples, the fluorescence decays were single exponential.

Figure 4 shows a comprehensive comparison of the JO and FL calculated radiative Tm^{3+} lifetimes and the experimental results obtained at 5 K and 300 K in the four hosts considered. It must be first noted that the results of the JO and FL calculations agree within the respective uncertainties of these calculations and that they show a reduction tendency for the Tm^{3+} radiative lifetimes in the NaTW sequence T = Gd → La → Y → Lu. This result is in accordance with the inverse dependence of the radiative lifetime on the oscillator strength, $\tau \sim f_{ED}^{-1}$, and therefore it agrees the results reported in Table SM2[31] and in Fig. 3. However, the experimental lifetimes obtained in the DW compounds with low (⩽0.2 at.%) Tm concentration do not show the same crystal host dependence. Considering the reasonable agreement between calculated and 300-K measured lifetimes, it may be qualitatively concluded that nonradiative

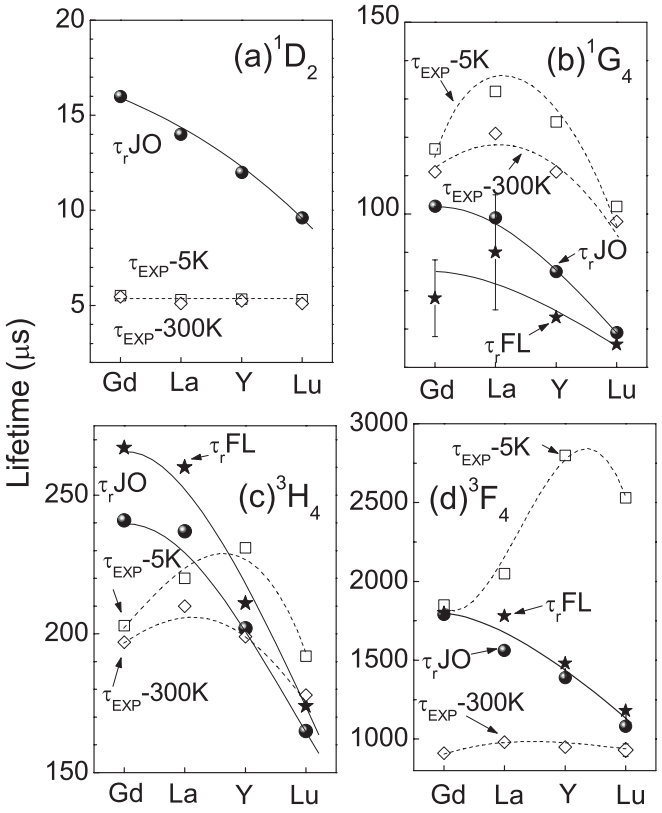

FIG. 4. Comparison of the $^1D_2$ (a), $^1G_4$ (b), $^3H_4$ (c), and $^3F_4$ (d) Tm^{3+} radiative lifetimes obtained by the JO (●) and FL (★) analyses in Tm:Na$T$$(WO_4)_2$ (T = Gd, La, Y, and Lu) with the fluorescence lifetimes measured at 5 K (□) and 300 K (◇) in the crystals with lowest Tm-concentration (Table I) and in 0.1 at.% Tm-doped polycrystalline powders for the $^3F_4$ case at room temperature.

de-excitation in the NaGdW and NaLaW crystals is stronger than in NaYW and NaLuW, for which such nonradiative processes are not pronounced or nonexistent, depending on the specific multiplet considered.

Similarly to the results presented in Fig. 4, upon temperature decrease an increase of the measured Tm^{3+} lifetimes above the calculated radiative values has been reported for the $^3F_4$ and $^3H_4$ Tm^{3+} multiplets in $LiLuF_4$[47] and in $Sr_5(PO_4)_3F$[48] crystals with low-energy phonon spectra. These changes have been ascribed either to a temperature-dependent diffusion coefficient for the cross-relaxation process involving both multiplets or to upconversion processes. Now we show that this behavior is observed also in oxide crystals, with much larger phonon energies, for most of the Tm^{3+} multiplets, and that the effect is more essential as the energy of the multiplet decreases. The origin of this temperature dependence of the Tm^{3+} experimental lifetimes is not fully understood in our present view, and it deserves further theoretical and experimental investigations. It seems to be related to intraionic interactions rather than to energy migration processes because it occurs for Tm density below 1×10^{19} cm^{-3}, with Tm-Tm distances beyond 30 Å, therefore interionic interactions are unlikely. In this regard, taking into account the mixed character of most Tm^{3+} multiplets, see Table IV, could be necessary.

Fluorescence dynamics, the $^3F_4$ case. The increase of the Tm concentration induces a reduction of the $^1D_2$, $^1G_4$, $^3H_4$, and $^3F_4$ PL lifetimes. This is associated to energy transfer and migration by Tm-Tm interactions. Details of these processes are given in Sec. V of the SM,[31] for brevity we considerer here only the case of the $^3F_4$ multiplet responsible of the PL near $\lambda \approx 2$ μm.

The measurement of the $^3F_4$ lifetime is complicated by the PL reabsorption. It is often argued that this effect can be ignored in samples with very low Tm concentration, i.e., $[Tm] < 5 \times 10^{19}$ cm^{-3}, for higher concentrations the pinhole method[49] or dispersion of powdered material in liquids with matched refractive index are used. Here we compare the results obtained by these methods.

Thin (<300 μm) plates were prepared for crystals with low (0.2 at.% in the melt) Tm concentration and for the pinhole method, applied for higher Tm doping levels. For comparison, we dispersed in ethylene glycol (EG, $n = 1.52$) microcrystalline DW ($n \approx 1.8$) powders obtained by single-crystal hand grinding in an agate mortar. In these cases the samples were excited at 796 nm, the maximum of the $^3H_6 \rightarrow {}^3H_4$ Tm^{3+} absorption, with an optical parametric oscillator. PL was detected at various wavelengths within the emission band, 1680–1850 nm (see Fig. SM10),[31] either with a PbS-photodiode at 300 K or with an InAs photovoltaic detector cooled to 77 K. The results obtained are shown in Fig. 5 (see filled symbols).

These results do not indicate any systematic dependence on the Tm concentration or crystal host, and the lifetimes measured for the lowest concentrations are larger than the radiative lifetimes calculated by the JO method; see Table VI. Performing an attempt to find a systematic variation of the results a large number of Tm-doped DW compositions prepared by solid-state reaction at 850 °C during 24 h were measured. The tetragonal scheelite-like phase of these powders was confirmed by powder θ-θ XRD scans. The $^3F_4$ lifetime of the polycrystalline powders dispersed in EG was measured in same conditions as for single crystals. The results are included in Fig. 5 as open symbols. In the T = La, Gd, and Y DW hosts the lifetime initially increases with Tm concentration, reaches a maximum and decreases monotonically with Tm concentration. In NaLuW the lifetime only decreases, but two ranges can be distinguished. The tendency changes at $[Tm] = 1–3 \times 10^{20}$ cm^{-3}. We ascribe this behavior to a competition between the apparent lifetime increase as a result of fluorescence reabsorption and the lifetime reduction due to nonradiative transitions induced by Tm-Tm energy transfer.

It is interesting to note that lifetimes measured in single crystals are generally larger than those obtained in polycrystalline powders, even those measured for 0.2 at.% Tm-doped crystals. This suggests that all $^3F_4$ lifetime measurements of single crystals are affected by reabsorption. In order to understand this situation, we studied the particle morphology of ground crystals and polycrystalline powders, in a FEI NOVA SEM scanning electron microscope (FE-SEM). Moreover, we employed a planetary ball mill to further reduce the particle size of ground crystals. Representative images of the particles are shown in Fig. SM15 of the SM.[31]

Crystals ground by hand are plates with a lateral size of about 10 μm and a side to height aspect ratio of ≈5–10,

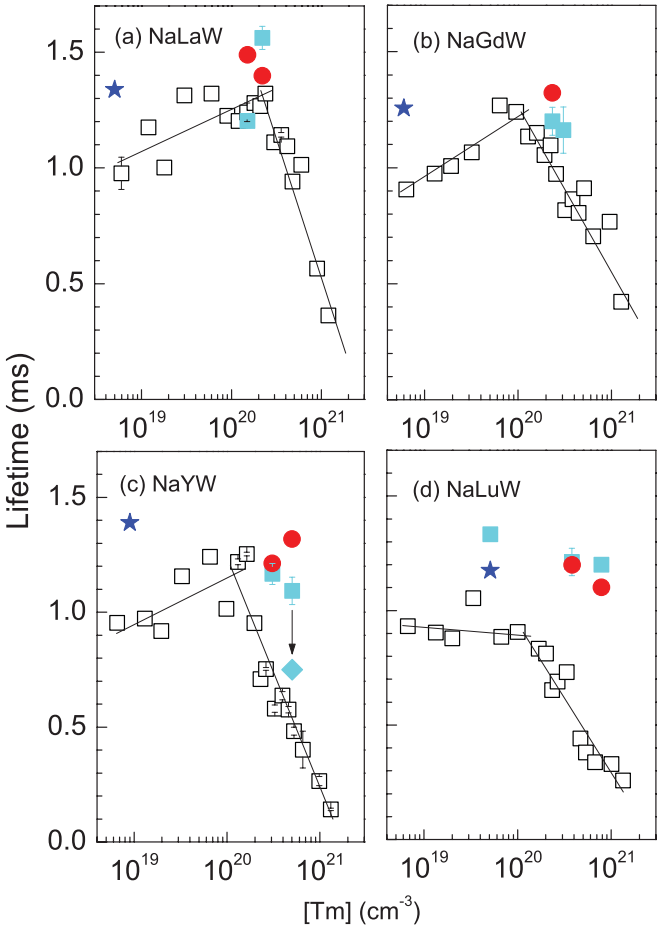

FIG. 5. (Color online) 300 K $^3F_4$ Tm^{3+} lifetime in Tm:Na$T$$(WO_4)_2$ DWs at different Tm concentrations. (a) T = La; (b) T = Gd; (c) T = Y; and (d) T = Lu. Thin plates of 0.2 at.% Tm-doped single crystals (★). Single-crystal plates measured by the pinhole method (●), powdered single crystals dispersed in EG (hand powdered, ■, ball milling, ◆), and polycrystalline powders synthesized by solid-state reaction and dispersed in EG (□), λ_{EXC} = 796 nm, λ_{EMI} = 1840 nm. The lines are guides to the eye.

this morphology arises from the cleavage of the crystals along the 001 plane giving rise to the flat faces observed. Particles prepared by solid-state reaction are pseudospheres with smooth curved surfaces and grain diameter in the 2- to 5-μm range, but they are highly sintered, forming aggregates with diameters in the 50- to 100-μm range. Finally, the particles prepared after 5 h or 15 h of crystal milling in the planetary ball mill have diameters in the 200- to 500-nm range, and they are strongly aggregated in clusters with a diameter of $\approx$10 μm. It must be noted that the large dimensions ($\gg$2 μm) of all these particles exclude a radiative lifetime modification induced by the EG medium.[50] The flat surfaces present in polished thin crystal plates and in microsized crystals obtained by hand grinding promote internal reflection of the PL emission and lead to an overestimation of the $^3F_4$ Tm^{3+} lifetime. This effect can be partially avoided by using particles with more spherical shapes. In fact the lifetimes measured in the powders obtained by ball milling are shorter than those measured in bulk (pinhole method) or hand-ground crystals and close to the measurement in pseudospheres obtained by solid-state reaction synthesis.

In summary, we believe that 0.1 at.% Tm-doped polycrystalline powers prepared by solid-state reaction and dispersed in EG provide near to true radiative $^3F_4$ Tm^{3+} lifetime values in NaTW compounds. These values are in the 0.9- to 1-ms range, i.e., slightly lower than the JO calculated values; see Table VI. The quantum efficiency of the radiative $^3F_4$ deexcitation, τ_{EXP}/τ_r, is 51, 63, 68, and 86% for NaTW T = Gd, La, Y, and Lu, respectively. As for other studied multiplets, nonradiative decay processes of $^3F_4$ are most pronounced in Gd- and La-based DW hosts; see Fig. 4(d).

V. LASER OPERATION

The cw laser operation characteristics of Tm-doped NaTW crystals at $\lambda \approx 1.95$ μm have been reported previously under Ti:sapphire laser pumping for T = Gd,[18] La,[16] and Lu,[25] as well as for DL pumping for T = Gd.[18] Here we present new laser results for Tm-doped NaYW and NaLuW crystals in comparison to those obtained in isostructural DWs.

A. Cross sections

As preliminary information on the laser properties of Tm^{3+} in NaYW, Fig. 6(a) shows the $^3H_4$ absorption cross sections associated with the optical pumping. The maximum absorption cross-section $\sigma_{ABS} = 3.73 \times 10^{-20}$ cm^2 occurs at 795.2 nm for σ-polarization. At the same wavelength, the absorption cross section for π-polarization is only, $\sigma_{ABS} = 1.44 \times 10^{-20}$ cm^2. The peak σ_{ABS} obtained for σ-polarization in NaYW is close to those obtained in NaLaW[16] and NaLuW,[25] $\sigma_{ABS} = 3.9 \times 10^{-20}$ cm^2, and 4.0×10^{-20} cm^2, respectively, and significantly larger than that observed in NaGdW, $\sigma_{ABS} = 2.9 \times 10^{-20}$ cm^2.[18] Table VII summarizes a comparison of these results in the four DW crystals considered along with the $^3F_4 \rightarrow {}^3H_6$ emission cross sections, σ_{EMI}, obtained at a laser wavelength.

Tm^{3+} lasers at $\lambda \approx 1.95$ μm operate as a quasi-three-level system, and therefore the efficiency depends critically on the population of the ground state. A first estimation of

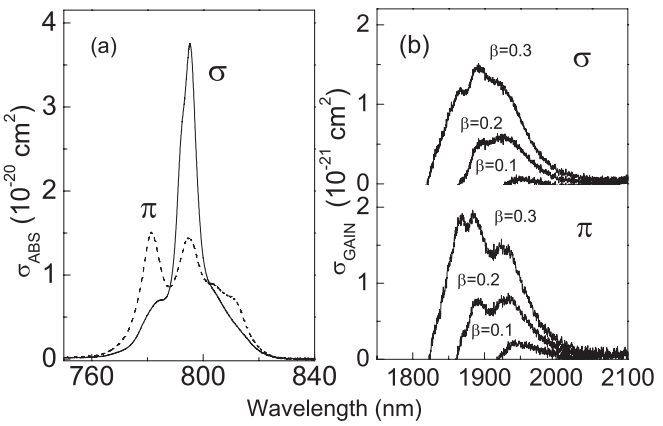

FIG. 6. Tm^{3+}:$NaY(WO_4)_2$ 300 K cross sections related to 2 μm lasing: (a) $^3H_6 \rightarrow {}^3H_4$ absorption cross sections for σ (continuous line) and π (dashed line) polarizations. (b) $^3F_4 \rightarrow {}^3H_6$ 300 K gain cross sections as a function of the inversion ratio, β.

TABLE VII. Spectroscopic parameters of Tm^{3+} in NaTW crystals at room temperature. Absorption, σ_{ABS}, and emission, σ_{EMI}, cross sections (10^{-20} cm^2) at the peak absorption wavelength, λ (nm) or at the naturally selected laser oscillation wavelength for 10% transmission output coupler, λ_L, (nm). For reference, gain cross sections, σ_{GAIN} (10^{-20} cm^2), have been estimated for $\beta = 0.3$. Partition function ratio, Z_l/Z_u, and energy gap, E_{zl} (cm^{-1}), between the upper ($^3F_4$) and lower ($^3H_6$) multiplets.

	$^3H_6 \rightarrow {}^3H_4$			$^3F_4 \leftrightarrow {}^3H_6$									
	σ,π	σ	π			σ				π			
Host	λ	σ_{ABS}	σ_{ABS}	Z_l/Z_u	E_{zl}	λ_L	σ_{ABS}	σ_{EMI}	σ_{GAIN}	λ_L	σ_{ABS}	σ_{EMI}	σ_{GAIN}
NaLaW	794.5	3.9	1.4	1.464	5605	1888	0.121	0.757	0.142	1880	0.147	0.826	0.145
NaGdW	795.0	2.9	1.2	1.436	5599	1895	0.108	0.717	0.140	1896	0.097	0.662	0.131
NaYW	795.2	3.7	1.4	1.448	5593	1938	0.073	0.543	0.112	1923	0.064	0.636	0.146
NaLuW	795.5	4.0	1.6	1.471	5591	1922	0.102	0.692	0.136	1923	0.096	0.592	0.110

the laser capability is provided by the gain cross section, $\sigma_{GAIN}(\lambda) = \beta\sigma_{EMI}(\lambda)$-$(1$-$\beta)\sigma_{ABS}(\lambda)$, where β represents the ratio of the Tm ions in the excited state to the total ion density. σ_{GAIN} is plotted in Fig. 6(b) for both polarizations indicating the expected oscillation wavelength in the absence of frequency selective elements in the laser cavity. Rather similar gain cross sections are found for both polarizations.

B. Laser results with Ti:sapphire pumping

Laser experiments were first performed under Ti:sapphire laser pumping at a pump wavelength $\lambda_{pump} = 796$ nm, i.e., close to the maximum absorption of the $^3H_4$ multiplet (see Table VII). Uncoated a-cut crystal plates were positioned at Brewster angle, between the two focusing mirrors of the astigmatically compensated X-type cavity (total length ~90 cm) as shown in Fig. 7(a).

Depending on the orientation of the crystal c-axis, both σ- and π-polarizations could be studied. The polarization of the pump laser was always in the same plane. M1, M2, and M3 mirrors were highly reflecting (HR; >99.9%) from 1800 to 2075 nm and antireflection (AR) coated on the rear side (highly transmitting for 780 to 1020 nm).

Plane output couplers [M4 in Fig. 7(a)] with transmission $T_{OC} = 1.5$, 3, 5, and 10% were used. At the position of the Tm-doped crystal, the pump spot had a Gaussian waist of 37 μm. The samples were fixed with one of their edges glued to a copper block without any special cooling.

Highly 5.03×10^{20} cm^{-3} (7.67 at.%) Tm-doped NaYW crystals were prone to damage because of their high pump absorption. Therefore, we studied the laser characteristics of the 3.07×10^{20} cm^{-3} (4.68 at.%) Tm-doped NaYW

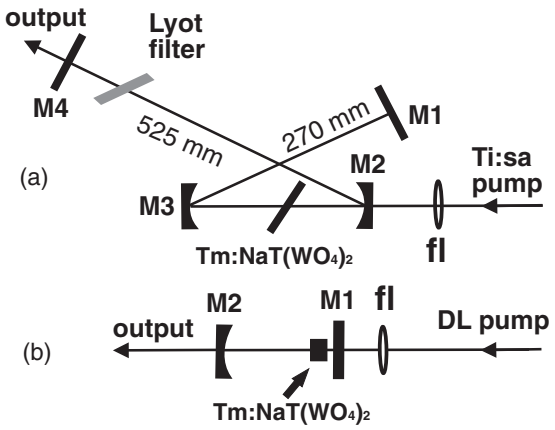

FIG. 7. (a) Cavity setup of the Tm:$NaY(WO_4)_2$ laser with Ti:sapphire laser pumping. fl: AR-coated focusing lens with $f = 70$ mm, M1: plane total reflector, M2-M3: RC = −100 mm mirrors, M4: plane output coupler. For tuning experiments a single plate birefringent filter (Lyot filter) was introduced into the cavity under Brewster angle. (b) Hemispherical cavity used for diode pumping the Tm:Na$T(WO_4)_2$ laser. M1: plane dichroic mirror. M2: RC = −50 mm output coupler.

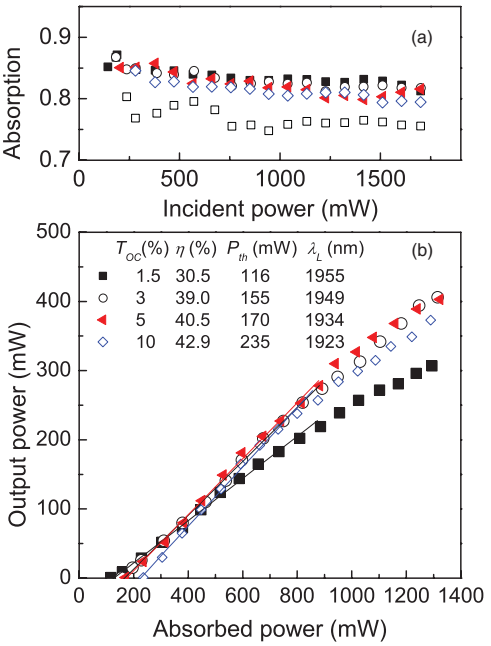

FIG. 8. (Color online) CW Tm-doped $NaY(WO_4)_2$ laser oriented for π-polarization (Tm^{3+}-doping: 3.07×10^{20} cm^{-3}, sample thickness 3.17 mm) under Ti-sapphire laser pumping ($\lambda_{pump} = 796.3$ nm). (a) Pump absorption under nonlasing (□), and lasing conditions with different output coupler transmissions, $T_{OC} = 1.5\%$ (■), 3% (○), 5%(◀), 10% (◇). (b) Input-output characteristics. The symbols show the experimental results, and the straight lines are fits for calculation of the slope efficiency η. The inset also includes the laser threshold in terms of absorbed pump power, P_{th}, and the laser wavelength, λ_L.

crystal. Because of the strong absorption anisotropy of the $^3H_4$ multiplet [see Fig. 6(a)], two different samples with thickness 3.17 and 1.26 mm were used for π- and σ-polarizations, respectively. Figs. 8(a) and 9(a) show the absorption of each sample. The absorption is bleached upon irradiation with the pump beam under nonlasing conditions. The stimulated emission recovers the absorption but cannot fully counterbalance the bleaching.

Figures 8(b) and 9(b) show the cw laser performance for π- and σ-polarizations, respectively. The output power scales linearly with the absorbed power up to ≈800 mW of absorbed power, and above there is a deviation from the linear dependence. The laser performance is rather similar for both polarizations. The slope efficiency (η, versus absorbed power) increases, and the laser emission wavelength decreases with increasing output coupler transmission. Thanks to the higher pump absorption, a maximum output power of 400 mW was obtained for π-polarization with a $T_{OC} = 3$–5%, but the maximum slope efficiency was $\eta \approx 42\%$ (for $T_{OC} = 10\%$) for both polarizations.

A single-plate intracavity Lyot filter (3-mm-thick quartz plate, optical axis 60° to the surface) was employed for tuning. Figure 10 shows the cw tuning range obtained using $T_{OC} = 3\%$ and incident pump power of $P_{inc} = 1.2$ W.

The tuning range obtained for π-polarization was 1854–2033 nm (179 nm) with a FWHM = 110 nm and for σ-polarization 1847–2069 nm (222 nm) with FWHM = 142 nm.

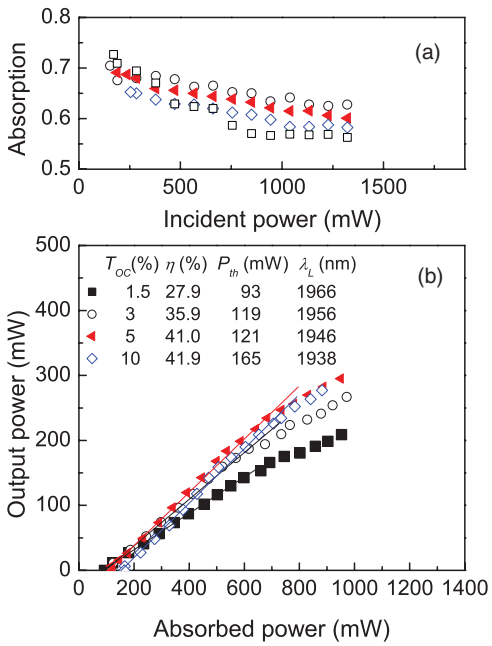

FIG. 9. (Color online) CW Tm-doped $NaY(WO_4)_2$ laser oriented for σ-polarization (Tm^{3+}-doping: 3.07×10^{20} cm^{-3}, sample thickness 1.26 mm) under Ti-sapphire laser pumping ($\lambda_{pump} = 796.3$ nm). (a) Pump absorption under nonlasing (□) and lasing conditions with different output coupler transmissions, $T_{OC} = 3\%$ (○), 5% (◀), 10% (◇). (b) Input-output characteristics. The symbols show the experimental results, and the straight lines are fits for calculation of the slope efficiency, η. The inset also includes the laser threshold in terms of absorbed pump power, P_{th}, and the laser wavelength, λ_L.

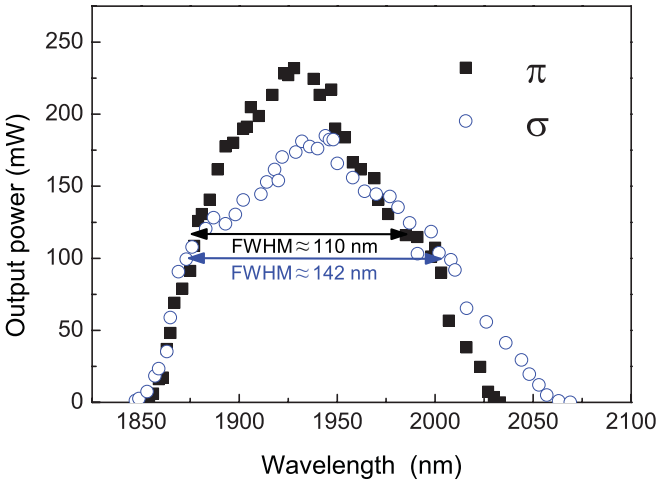

FIG. 10. (Color online) Spectral tunability of the cw Tm:$NaY(WO_4)_2$ laser (Tm^{3+}-doping 3.07×10^{20} cm^{-3}) under Ti-sapphire laser pumping and using a $T_{OC} = 3\%$ output coupler. The sample thickness was 3.17 mm for π-polarization and 1.26 mm for σ-polarization. The incident pump power P_{inc} was 1.2 W at $\lambda_{pump} = 796.3$ nm. The FWHM of the tuning curves are indicated in the figure.

These tuning ranges are the broadest obtained for this class of Tm-doped DW crystals.

C. Laser results under DL pumping

In that case the pump source was a fiber-coupled DL. The fiber had a core diameter of 200 μm and a NA = 0.22. The spectral emission of the DL ranged from 800 to 804 nm, depending on temperature and output power. For the present study, the pump wavelength was set at 801 nm. The unpolarized output of the pump beam was focused by a $f = 30$-mm lens to a spot size of 175 μm. A two mirror hemispherical resonator with a length of 49 mm [Fig. 7(b)] was used. The plane pump mirror (M1) was AR coated for the range 770–1050 nm and HR coated in the 1800- to 2075-nm range. Output couplers (M2) with transmissions $T_{OC} = 1.5$, 3, and 5% in the range 1820–2050 nm and radius of curvature of −50 mm were used. The crystals were positioned in the vicinity of the pump focus at normal incidence. The samples were water cooled in a copper holder. Two *a*-cut Tm-doped NaTW crystals were studied under DL pumping: Tm:NaYW (3.07×10^{20} cm^{-3} Tm^{3+}-doping, thickness: 2.7 mm) and Tm:NaLuW (3.8×10^{20} cm^{-3} Tm^{3+}-doping, thickness: 1.7 mm).

Figure 11 shows the Tm-doped DW laser performance under DL pumping. For Tm:NaYW crystal, the highest output power obtained was 207 mW for $T_{OC} = 5\%$ with a slope efficiency of $\eta = 7.5\%$ with respect to incident power. The lowest laser threshold corresponded to 730 mW of incident pump power. For the Tm:NaLuW crystal, the maximum output power obtained was 234 mW for $T_{OC} = 3\%$ at an incident power of 2.45 W. The same T_{OC} also provided the highest slope efficiency of $\eta = 14.6\%$.

Figure 12 shows the spectral distribution of the free running laser emission for the DL pumped Tm:NaYW crystal. As for Ti:sapphire laser pumping, the laser wavelength shifted to

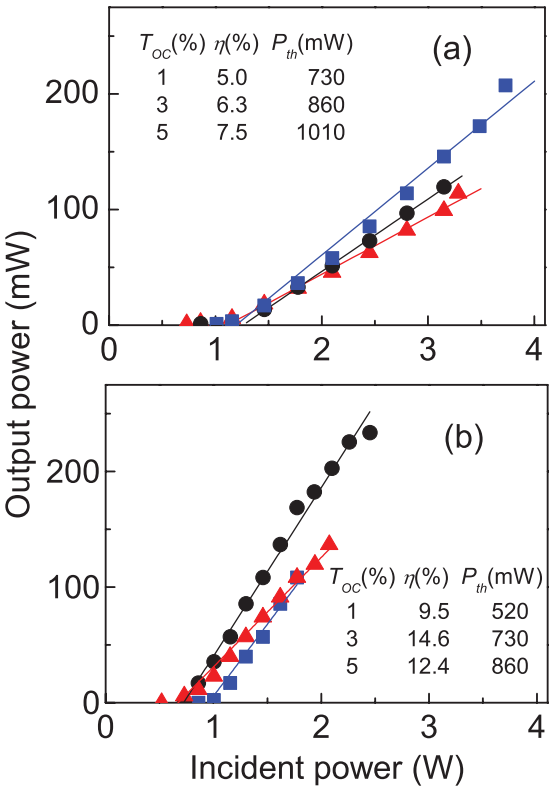

FIG. 11. (Color online) Input-output characteristics of cw Tm-doped DW lasers with DL pumping. (a) 3.07×10^{20} cm^{-3} Tm-doped $NaY(WO_4)_2$, sample thickness: 2.7 mm. (b) 3.8×10^{20} cm^{-3} Tm-doped $NaLu(WO_4)_2$, sample thickness: 1.7 mm. $T_{OC} = 1.5\%$ (▲), $T_{OC} = 3\%$ (●) and $T_{OC} = 5\%$ (■).

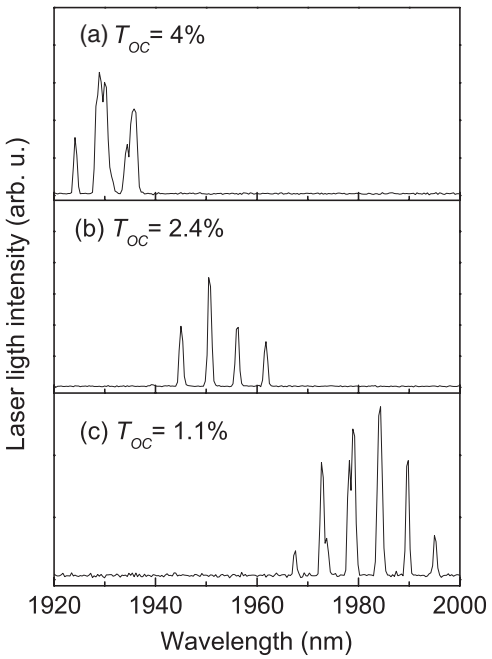

FIG. 12. Spectra of the free-running Tm:$NaY(WO_4)_2$ laser for different output coupler transmissions, T_{OC}. (Tm-doping: 3.07×10^{20} cm^{-3}).

shorter values with increasing T_{OC}. The higher gain necessary to compensate for the increased losses in the cw regime requires higher inversion ratio for which the position of the gain cross-section maximum moves to shorter wavelengths; see Fig. 6(b).

The output spectrum of the Tm:NaYW laser consists of discrete lines not related to the longitudinal mode structure. The spectral extension depends on T_{OC}, as lower the transmission, as broader the spectral emission. This is related to the reduced loss (lower threshold) for lower output coupling and to the flat gain curves at low inversion level [Fig. 6(b)]. Thus, for output coupling of 1.1%, the spectral emission is ∼25 nm broad, for $T_{OC} = 2.4\%$, it is ∼15 nm, and for $T_{OC} = 4\%$ it is ∼10 nm. These results together with the broad spectral cw tuning range (>200 nm) suggest a high potential of the studied Tm-doped DW crystals for the generation of ultrashort laser pulses.

The polarization of the laser emission near 2 μm showed a dependence on T_{OC}. Although the pump beam was not polarized, the birefringent NaYW crystal naturally selected the π-polarization. The latter exhibits a slightly higher gain compared to the σ-polarization, as shown in Figure 6(b). Due to the decrease of the absolute gain difference between π- and σ-polarization with reduced inversion level (reduced output coupler transmission), the emission is no more pure π-polarization. In the case of Tm:NaYW for higher coupling, $T_{OC} = 5\%$, the polarization degree was 10:1 with the predominant gain for π-polarization. Lowering the output coupling to $T_{OC} = 3\%$, the polarization degree is reduced to 2:1 with still the π-polarization dominating. Finally, for the lowest coupling ($T_{OC} = 1.5\%$), a dominating polarization could not be distinguished.

VI. CONCLUSIONS

Despite of the isostructural character and close unit cell parameters of tetragonal $NaT(WO_4)_2$ (T = La, Gd, Y, and Lu) crystals, the spectroscopic properties of Tm^{3+} in these hosts follow well-defined trends. The preferential occupancy of 2d sites by trivalent cations and larger bond anisotropy are associated with narrower Tm^{3+} transition linewidths in NaLaW in comparison to the other considered Na-based DWs with close to random distribution in 2d and 2b sites (NaGdW and NaLuW) or even in NaYW with preferential occupancy of the 2b site.

The spectroscopic properties of Tm^{3+} in NaTW crystals agree with a Γ_2 irreducible representation for the ground $^3H_6(0)$ Stark level. On the basis of 5 K optical absorption and photoluminescence measurements as well as on a CF parametrization, the full list of Stark level energies up to the $^3P_0$ multiplet has been obtained for each of the four considered crystals. This enabled the calculation of reliable values for the partition function of multiplets involved in Tm^{3+} laser transitions.

The comparison of the radiative lifetime trends obtained by the JO or by the FL methods with the experimetal values obtained in crystals with low (<1 × 10^{19} cm^{-3}) content of Tm suggests that nonradiative losses are larger in NaGdW and NaLaW crystals.

The comparison of the laser operation results obtained in this work with previous results in other NaTW crystals shows that under similar room-temperature and pump conditions, the

highest output powers for true cw laser operation near 2 μm are achieved in Tm-doped NaYW, 400 mW with slope efficiency $\eta = 42\%$ and in Tm-doped NaLuW, 435 mW with $\eta = 50\%$. These values are significantly higher than those obtained with Tm-doped NaGdW and NaLaW crystals. The spectral tuning range of NaTW (T = Gd, Y, or Lu) spans over ≈200 nm in the 1800- to 2050-nm region. Due to the additional Czochralski growth advantage of NaYW over NaLuW, the former seems the best choice for implementation of mode-locked femtosecond lasers operating in the 2 μm spectral range.

ACKNOWLEDGMENTS

Work supported by the Spanish government under projects MAT2008-06729-C02 and MAT2011-29255-C02. M. Rico is supported by Grant No. RYC2005-1922.

*cezaldo@icmm.csic.es

[1] J. Ganem, J. Crawford, P. Schmidt, N. W. Jenkins, and S. R. Bowman, Phys. Rev. B **66**, 245101 (2002).
[2] V. Sudesh and J. A. Piper, IEEE J. Quantum Electron. **36**, 879 (2000).
[3] A. A. Kaminskii, *Crystalline Laser: Physical Processes and Operating Schemes* (CRC Press, New York, 1996), Chap. 1, p. 46.
[4] R. Allen, L. Esterowitz, and I. Aggarwal, IEEE J. Quantum Electron. **29**, 303 (1993).
[5] S. Sanders, R. G. Waarts, D. G. Mehuys, and D. F. Welch, Appl. Phys. Lett. **67**, 1815 (1995).
[6] R. Scheps, Prog. Quantum Electron. **20**, 271 (1996).
[7] V. A. French, R. R. Petrin, R. C. Powell, and M. Kokta, Phys. Rev. B **46**, 8018 (1992).
[8] A. Brenier, L. C. Courrol, C. Pédrini, C. Madej, and G. Boulon, Phys. Rev. B **49**, 881 (1994).
[9] X. Han, F. Fusari, M. D. Serrano, A. A. Lagatsky, J. M. Cano-Torres, C. T. A. Brown, C. Zaldo, and W. Sibbett, Opt. Express **18**, 5413 (2010).
[10] M. C. Pujol, F. Güell, X. Mateos, J. Gavaldà, R. Solé, J. Massons, M. Aguiló, F. Díaz, G. Boulon, and A. Brenier, Phys. Rev. B **66**, 144304 (2002).
[11] R. C. Stoneman and L. Esterowitz, Opt. Lett. **15**, 486 (1990).
[12] V. Petrov, F. Güell, J. Massons, J. Gavaldà, R. M. Solé, M. Aguiló, F. Díaz, and U. Griebner, IEEE J. Quantum Electron. **40**, 1244 (2004).
[13] G. Galzerano, F. Cornacchia, D. Parisi, A. Toncelli, M. Tonelli, and P. Laporta, Opt. Lett. **30**, 854 (2005).
[14] A. García-Cortés, J. M. Cano-Torres, M. D. Serrano, C. Cascales, C. Zaldo, S. Rivier, X. Mateos, U. Griebner, and V. Petrov, IEEE J. Quantum Electron. **43**, 758 (2007).
[15] A. A. Lagatsky, X. Han, M. D. Serrano, C. Cascales, C. Zaldo, S. Calvez, M. D. Dawson, J. A. Gupta, C. T. A. Brown, and W. Sibbett, Opt. Lett. **35**, 3027 (2010).
[16] J. M. Cano-Torres, X. Han, A. García-Cortés, M. D. Serrano, C. Zaldo, F. J. Valle, X. Mateos, S. Rivier, U. Griebner, and V. Petrov, Mater. Sci. Eng. B **146**, 22 (2008).
[17] Y. Wei, C. Tu, H. Wang, F. Yang, G. Jia, Z. You, J. Li, Z. Hu, and Y. Wang, Appl. Phys. B **86**, 529 (2007).
[18] J. M. Cano-Torres, M. D. Serrano, C. Zaldo, M. Rico, X. Mateos, J. Liu, U. Griebner, V. Petrov, F. J. Valle, M. Galán, and G. Viera, J. Opt. Soc. Am. B **23**, 2494 (2006).
[19] E. V. Zharikov, D. A. Lis, A. V. Popov, K. A. Subbotin, S. N. Ushakov, A. V. Shestakov, and I. Razdobreev, Quantum Electron. **36**, 515 (2006).
[20] F. A. Bolschikov, G. M. Kuz'micheva, D. A. Lis, Yu. M. Papin, A. V. Popov, P. A. Ryabochkina, V. B. Rybakov, V. G. Senin, V. A. Smirnov, K. A. Subbotin, Yu. K. Voron'k, V. V. Voronov, and E. V. Zharikov, J. Cryst. Growth **311**, 4171 (2009).
[21] F. Song, L. Han, C. Zou, J. Su, K. Zhang, L. Yan, and J. Tian, Appl. Phys. B **86**, 653 (2007).
[22] J. Su, F. Song, H. Tan, L. Han, F. Zhou, J. Tian, G. Zhang, Z. Cheng, and H. Chen, J. Phys. D **39**, 2094 (2006).
[23] F. Song, J. Su, H. Tao, L. Han, B. Fu, J. Tian, G. Zhang, Z. Cheng, and H. Chen, Opt. Commun. **241**, 455 (2004).
[24] C. Sun, F. Yang, T. Cao, Z. You, Y. Wang, J. Li, Z. Zhu, and C. Tu, J. Alloys Compd. **509**, 6987 (2011).
[25] X. Han, J. M. Cano-Torres, M. Rico, C. Cascales, C. Zaldo, X. Mateos, S. Rivier, U. Griebner, and V. Petrov, J. Appl. Phys. **103**, 083110 (2008).
[26] R. D. Shannon, Acta Crystallogr. A **32**, 751 (1976).
[27] F. J. Valle, P. Ortega, A. de Pablos, C. Zaldo, F. Esteban-Betegón, and M. D. Serrano, X-Ray Spectrometry **38**, 287 (2009).
[28] C. Cascales, M. D. Serrano, F. Esteban-Betegón, C. Zaldo, R. Peters, K. Petermann, G. Huber, L. Ackermann, D. Rytz, C. Dupré, M. Rico, J. Liu, U. Griebner, and V. Petrov, Phys. Rev. B **74**, 174114 (2006).
[29] X. Han, A. García-Cortés, M. D. Serrano, C. Zaldo, and C. Cascales, Chem. Mater. **19**, 3002 (2007).
[30] M. Rico, A. Méndez-Blas, V. Volkov, M. A. Monge, C. Cascales, C. Zaldo, A. Kling, and M. T. Fernández-Díaz, J. Opt. Soc. Am. B, **23**, 2066 (2006).
[31] See Supplemental Material at http://link.aps.org/supplemental/10.1103/PhysRevB.84.174207 for detailed x-ray diffraction data, additional optical spectroscopic information and images of the powders used for lifetime characterization are given along with a prospective of the crystal potential for mode-locked laser operation.
[32] R. D. Shannon, P. S. Gummerman, and J. Chenavas, Am. Mineral. **60**, 714 (1975) [http://www.minsocam.org/ammin/AM60/AM60_714.pdf].
[33] D. E. Wortman, C. A. Morrison, and R. P. Leavitt, Phys. Rev B **12**, 4780 (1975).
[34] W. T. Carnall, G. L. Goodman, K. Rajnak, and R. S. Rana, J. Chem. Phys. **90**, 3443 (1989).
[35] M. Rico, V. Volkov, C. Cascales, and C. Zaldo, Chem. Phys. **297**, 73 (2002).
[36] C. Cascales and C. Zaldo, Chem. Mater. **18**, 3742 (2006).
[37] A. Méndez-Blas, M. Rico, V. Volkov, C. Zaldo, and C. Cascales, Phys. Rev. B **75**, 174208 (2007).
[38] B. R. Judd, Phys. Rev. **127**, 750 (1962).
[39] G. S. Ofelt, J. Chem. Phys. **37**, 511 (1962).
[40] H. Wang, G. Jia, F. Yang, Y. Wei, Z. You, Y. Wang, J. Li, Z. Zhu, X. Lu, and C. Tu, Appl. Phys. B **83**, 579 (2006).
[41] X. Lu, Z. You, J. Li, Z. Zhu, G. Jia, B. Wu, and C. Tu, Opt. Mater. **29**, 849 (2007).

[42] A. García-Cortés, C. Cascales, A. de Andrés, C. Zaldo, E. V. Zharikov, K. A. Subbotin, S. Bjurshagen, V. Pasiskevicius, and M. Rico, IEEE J. Quantum Electron. **43**, 157 (2007).
[43] A. García-Cortés, J. M. Cano-Torres, X. Han, C. Cascales, C. Zaldo, X. Mateos, S. Rivier, U. Griebner, V. Petrov, and F. J. Valle, J. Appl. Phys. **101**, 063110 (2007).
[44] A. Méndez-Blas, M. Rico, V. Volkov, C. Zaldo, and C. Cascales, Mol. Phys. **101**, 941 (2003).
[45] B. F. Aull and H. P. Jenssen, IEEE J. Quantum Electron. **18**, 925 (1982).
[46] D. E. McCumber, Phys. Rev. A **136**, 954 (1964).
[47] F. Cornacchia, D. Parisi, and M. Tonelli, IEEE J. Quantum Electron. **44**, 1076 (2008).
[48] L. J. Richardson, C. E. Bonner Jr., J. Lewis, G. B. Loutts, W. J. Rodriguez, and B. M. Walsh, J. Lumin. **109**, 129 (2004).
[49] H. Kühn, S. T. Fredrich-Thornton, C. Kränkel, R. Peters, and K. Petermann, Opt. Lett. **32**, 1908 (2007).
[50] R. S. Meltzer, S. P. Feofilov, B. Tissue, and H. B. Yuan, Phys. Rev. B **60**, R14012 (1999).